Collision processes in atoms and molecules using effective potentials

Alejandra M.P. Mendez , Darío M. Mitnik , and Jorge E. Miraglia

Instituto de Astronomía y Física del Espacio, Universidad de Buenos Aires – Consejo Nacional de Investigaciones Científicas y Técnicas, Buenos Aires, Argentina

April 1, 2019

Contents

Abstract

We investigate the feasibility of using pseudopotentials to generate the bound and continuum orbitals needed in collisional calculations. By examination of several inelastic processes, we demonstrate the inconveniences of this approximation. Instead, we prescribe the usage of effective potentials obtained with the Depurated Inversion Method (DIM), which is described in this work. We also extended this method for molecular systems. Calculations of single photoionisation and proton–impact ionisation with DIM show good agreements with experimental results.

1 Outline

Inelastic transition calculations require the representation of the bound and continuum states involved in the collisional processes. The hypothetical existence of an effective one–electron local potential accounting for these states would allow to generate in a simpler way the orthogonal wavefunctions for the interacting particles. This should include detailed nl–orbital potentials, a feature missing in most of the standard density functional methods. The idea of replacing a many–body, nonlocal interaction by an effective one–electron equation opens up the possibility of studying extremely complex systems with high accuracy. However, this is not a simple task.

In this context, one clever idea emerge from the pseudopotential approximation, in which all the complexity of the wavefunctions near the core – that normally consumes a huge numerical effort –, is avoided. For instance, density functional theory codes using pesudopotentials, such as the PARSEC for example [**?**, **?**], permit to use an equally–spaced grid involving a relatively small number of points. Otherwise, the use of realistic potentials describing properly the nucleus Coulomb potential, requires a high density of points concentrated at the origin to describe precisely what the pseudopotentials cast aside. Thus, if this approach is applicable in the field of collisions theory, one would save enormous amount of computational resources. In this article, we explore the possibility of using pseudopotentials within the single electron model to calculate inelastic transitions. Single photoionization, excitation, ionization and electron capture were calculated in first perturbative order. We found two important drawbacks in this applications. First, the range of validity is restrained to very small momentum transfers. Second, the internal information of the wavefunctions can play a very important role, such as the cusp conditions in the processes of electron capture and ionization.

In previous works [**?**, **?**, **?**], we developed the Depurated Inversion Method (DIM), allowing to obtain accurate effective potentials by substituting the coupled multielectron equations into a Kohn–Sham type equation. In a first step, the corresponding effective potential is obtained through inversion of this equation. Next, a careful optimisation of this potential is carried on, eliminating poles, and imposing

analytically, the appropriate boundary conditions. In that way, the DIM potentials are parametrized in simple analytical expressions. In the present work, we show how these DIM potentials overcome the deficiencies of the pseudopotentials, calculating the cross sections for inelastic problems.

Finally, an extension of the DIM method for simple molecular system is developed, providing a new parameteric expression and results for collisional processes. An implementation example is given for the methane molecule.

2 Theory

2.1 Pseudopotentials

The pseudopotential (PP) method consists of replacing the Coulomb potential in the many–electron system Hamiltonian with a smooth function so that the electron wavefunctions oscillating rapidly in the core region are replaced by nodeless pseudo–orbitals having the correct energy and the same outer range properties. In general, the pseudopotentials V_{PP} can be defined through a pseudo–charge Z_{PP} as

$$V_{\text{PP}}(r) = -\frac{Z_{\text{PP}}(r)}{r}\,, \tag{1}$$

$$Z_{\text{PP}}(r) = \begin{cases} f(r), & r \le r_c \\ 1, & r > r_c \end{cases}\,, \tag{2}$$

where r_c is a cutoff radius that separates the core, $r \le r_c$, from the valence region, $r > r_c$, of the target and $f(r)$ is a continous function with a constant value at the origin. Fig. **??** illustrates a pseudopotential (solid line) and its corresponding pseudo–wavefunction for the $3s$ orbital of argon. The one–electron Hartree–Fock wavefunction is included with a dashed line. The pseudo–wavefunction agrees with the HF orbital only in the outer region, loosing all infomation about the atomic structure close to the origin.

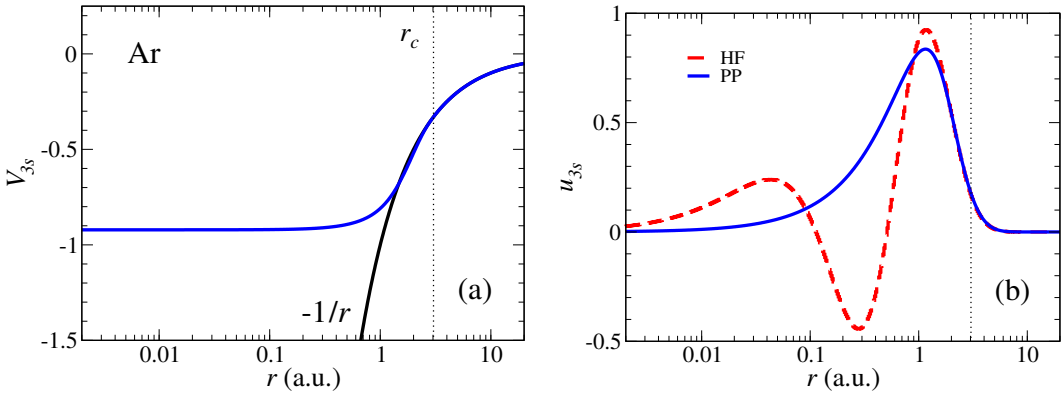

Figure 1: (a) Pseudopotential, (b) pseudo–wavefunction and HF orbital for the $3s$ orbital of argon.

In Section **??**, we analyze the feasibility of implementing PPs in collisional processes calculations for two simple atomic cases: hydrogen and lithium. For each atom, the following pseudopotentials are examined

Name	Source	Type	Ref.
A	ABINIT	GGA	[**?**, **?**]
P	PARSEC	Troullier Martins	[**?**, **?**].

(3)

Although there is no electronic core for hydrogen orbitals, it can still be readily described by the pseudopotential approximation. In fact, the hydrogen pseudopotentials from (**??**) reproduce the exact orbitals very accurately.

We will now proceed to examine closely the pseudo–charges and its one–electron solutions for the lithium atom. First, we study the spatial and momentum representation of the pseudo–charges. The momentum–space equivalent of $Z(r)$ is given by the Fourier transform

$$\widetilde{Z}(k) = \frac{1}{\sqrt{2\pi}} \int_{-\infty}^{+\infty} Z(r)\, e^{-ikr}\, dr\,. \tag{4}$$

The pseudo–charges from (**??**) for the $2s$ orbital of lithium are illustrated in Fig. **??**. For comparison, we include the potential attained from implementing the Depurated Inversion Method described in Section **??**. The pseudo–charges vanish at the origin, avoiding the divergence of the Coulomb potential. However, this feature comes at a price: the pseudo–charges in the spatial representation are repulsive around r =1 a.u. and their momentum picture fails to represent the target for high k, showing an incorrect oscillatory behaviour for values greater than $k_c = (2\pi r_c)^{-1} \sim 0.7$ a.u..

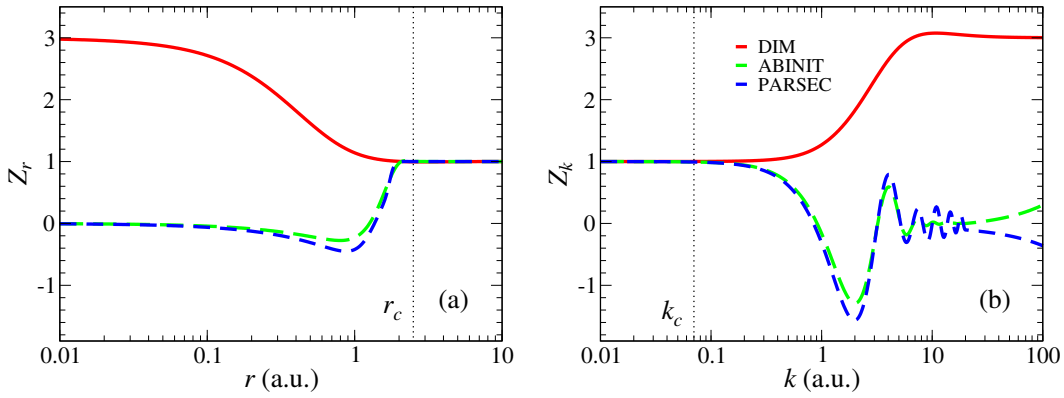

Figure 2: Pseudo and DIM charges for the $2s$ orbital of lithium. (a) Spatial and (b) momentum representation.

Secondly, we inspect the behaviour of the bound pseudo–orbitals obtained from solving the one–electron Schrodinger equation with a pseudopotential. As usual, the bound state wavefunctions can be written as

$$\psi_{nlm}(\mathbf{r}) = \frac{u_{nl}(r)}{r} Y_l^m(\hat{r})\,, \tag{5}$$

where $u_{nl}(r)$ are the reduced radial wavefunctions and $Y_l^m(\hat{r})$ are th spherical harmonics. Similarly, the Fourier transform of these functions are given by

$$\widetilde{\psi}_{nlm}(\mathbf{k}) = \frac{\chi_{nl}(k)}{k} Y_l^m(\hat{k})\,. \tag{6}$$

The spatial and momentum representation of the $2s$ radial pseudo–wavefunctions of lithium corresponding to the pseudo–charges from (**??**) are displayed in Fig. **??**. Although the pseudo–orbitals are very different than the HF $2s$ wavefunction, the transformed $\chi(k)$ seems to have similar characteristics. However, a closer inspection of the tail region of these functions (see the inset of the figure) show the existence of several nodes. We will see later that these discrepancies introduce significant consequences in the cross sections for most of the collisional processes examined.

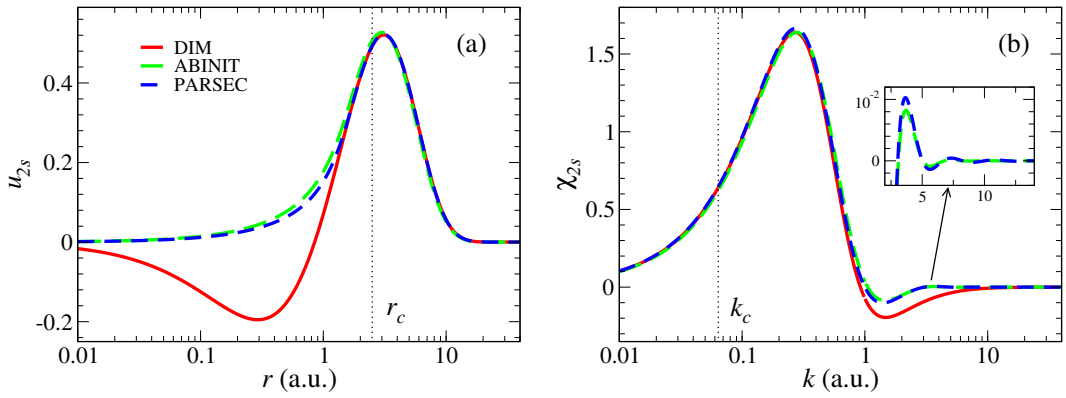

Figure 3: Pseudo and DIM bound state wavefunction in (a) spatial and (b) momentum representation for the $2s$ orbital of lithium.

Finally, the pseudopotential approach not only affects the representation of the bound orbitals, but also determines the form of the continuum wavefunctions. For large r, the free state orbitals of an electron in presence of a Coulomb potential can be written as

$$u_{kl}(r) \rightarrow \sin\left(kr - l\frac{\pi}{2} - \eta \ln 2kr + \sigma_l + \delta_l\right) , \tag{7}$$

where k is the particle wave number, η is Sommerfeld's parameter, σ_l is the Coulomb phase shift and δ_l is the wave phase shift with respect to the Coulomb wave.

Comparisons between the DIM (solid line) and the pseudo (dashed) free ks wavefunctions for lithium are shown in Fig. **??**, close to the origin (left) and asymptotically (right). The pseudo and DIM wavefunctions behave similarly far away from the nucleus. The asymptotic phase shift Δ accounts for the differences between the potentials. As the energy of the free electron increases, Δ diminishes. However, the orbitals in the core region are different even with increasing energy; the first maximum of the DIM wavefunctions are consistently smaller than of the pseudo–orbitals, which is understood since the Coulomb–type attraction of the nuclei is stronger than the pseudopotential in that region.

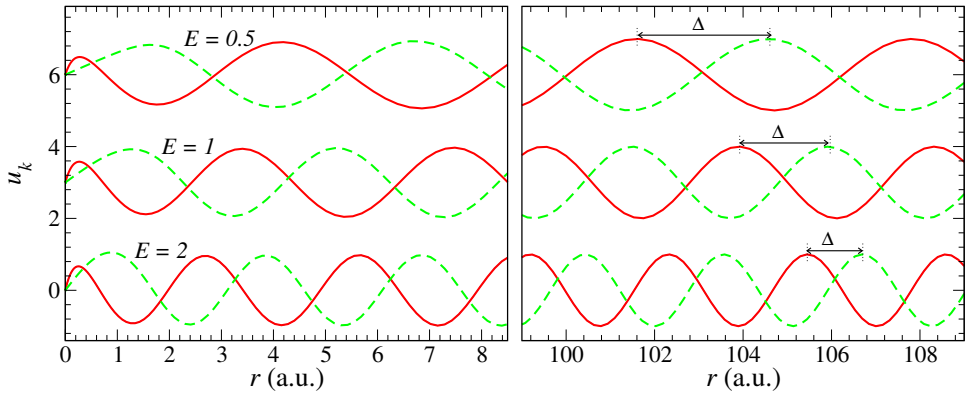

Figure 4: Continuum wavefunctions with energies E near the origin (left) and in the asymptotic region (right), calculated with the DIM potential (solid line) and the ABINIT pseudopotential (dashed line).

2.2 Depurated Inversion Method potentials

The Depurated Inversion Method [**?**, **?**, **?**] consists of assuming that the many–electron atom orbitals can be represented by the solution of Kohn–Sham type equations, in which the nl effective potentials are

given by

$$V_{nl}(r) = \frac{1}{2}\frac{1}{u_{nl}(r)}\frac{d^2u_{nl}(r)}{dr^2} - \frac{l(l+1)}{2r^2} + \varepsilon_{nl}\,, \tag{8}$$

where u_{nl} and ε_{nl} are the nl orbital wavefunctions and energies, respectively. In this work, the atomic structure is approximated with the Hartree–Fock method, which is computed with the HF codes by C. F. Fischer [**?**] and the NRHF code by W. Johnson [**?**]. The computation of Eq. (**??**) poses various numerical problems. The nodes and asymptotic decay of the wavefunctions $u_{nl}(r)$ introduce significant numerical errors in the inversion procedure (see Ref. [**?**] for further details). The nodes of the orbitals produces huge unphysical poles, while the rapid asymptotic decay of the internal wavefunctions generates large divergences in the tail region of the potentials. The Depuration method is implemented to tackle these unphysical features. An effective potential with a Coulomb–type shape $V_r(r) = -Z_r(r)/r$ is defined, and we enforce the correct boundary conditions fitting the inverted potential with the following analytical expression

$$Z_r(r) = \sum_{j=1}^{n} z_j e^{-\alpha_j r}(1+\beta_j r) + 1 \longrightarrow \begin{cases} Z_N, & r \to 0 \\ 1, & r \to \infty \end{cases} \tag{9}$$

where $\sum z_j = Z_N - 1$. Afterwards, the parameters are optimised to reproduce the HF values accurately.

3 Collisional processes in atoms

The most significative advantage of the pseudopotential method is its symplicity. However, it is worth to determine the validity of this approach for computing collisional processes. In this Section, we perform a thorough examination of the pseudo–potentials for hydrogen and lithium by comparing the cross sections of four inelastic processes: proton–impact excitation, proton–impact ionisation, charge exchange and photoionisation. The initial and final states of the targets are obtained by solving the corresponding Schrödinger equation. For the hydrogen atom, we compare the pseudopotential results with the exact analytical solutions. Furthermore, in order to asses the aplicability of the Depurated Inversion Method, we compute the photoionisation of more complex many–electron atoms and compare our findings with experimental data.

3.1 Proton–Impact Excitation

The proton–impact excitation of target X is defined as

$$\mathrm{H}^+ + X \to \mathrm{H}^+ + X^*\,. \tag{10}$$

The excitation cross section σ of the target from the initial bound state ψ_i to the excited state ψ_f may be written as

$$\sigma = \frac{\mu^2}{4\pi^2}\frac{k_f}{k_i}\int |T_{fi}|^2\, d\Omega\,, \tag{11}$$

where μ is the reduced mass of the proton–atom system, $\mathbf{k}_i$ and $\mathbf{k}_f$ are the initial and final relative momentum, and

$$T_{fi} = \langle \psi_f | V | \psi_i \rangle \tag{12}$$

is the transition matrix or T–matrix. If the initial and final state of the transition are described by the Hartree–Fock method, the orbitals will give the correct high energy limit in the first order approximation (this is not the case for the charge exchange process). Hence, we will concentrate our computing efforts in the first perturbative order of the transition matrix element through the first Born (FB) approximation, given by

$$T_{fi}^{\mathrm{FB}} = \widetilde{V}(\mathbf{p}) F_{fi}(\mathbf{p})\,. \tag{13}$$

The term $F_{fi}(\mathbf{p})$ is the form–factor

$$F_{fi}(\mathbf{p}) = \frac{1}{(2\pi)^{3/2}}\int \widetilde{\psi}_f^*(\mathbf{k})\widetilde{\psi}_i(\mathbf{k}+\mathbf{p})\, d\mathbf{k}\,, \tag{14}$$

where $\mathbf{p}$ is the momentum transfer vector

$$\mathbf{p} = p_{\min}\hat{\mathbf{v}} + \boldsymbol{\eta}\,, \tag{15}$$

$$p_{\min} = \frac{\varepsilon_f - \varepsilon_i}{v} \to \begin{cases} \infty, & v \to 0 \\ 0, & v \to \infty \end{cases}\,, \tag{16}$$

$\hat{\mathbf{v}}$ is the ion velocity, $\boldsymbol{\eta}$ is the transversal momentum transfer, so that $\hat{\mathbf{v}}\cdot\boldsymbol{\eta} = 0$, whereas ε_i and ε_f are the binding energies corresponding to the initial and final state.

The first Born proton–impact excitation cross sections of hydrogen and lithium from the ground states are shown in Fig. **??**. The pseudopotential results for the $n = 2$ and $n = 3$ final states of hydrogen agree excellently with the analytical expression. For lithium, the pseudopotential cross sections agree in a broad velocity range with the DIM calculations, except for low proton–impact velocities. This disagreement arises from the form factor. For low impact velocities, the momentum transfer vector is large (**??**). As discussed earlier, the bound momentum orbital $\widetilde{\psi}(\mathbf{k}+\mathbf{p})$ is not properly described by the pseudopotentials at this region. An alternative expression for the form factor can be considered by implementing the peaking approximation

$$F_{fi}(\mathbf{p}) \sim \widetilde{\psi}_i(\mathbf{p})\widetilde{\psi}_f^*(0) + \widetilde{\psi}_f(\mathbf{p})\widetilde{\psi}_i^*(0)\,. \tag{17}$$

Therefore, in order to have the correct form factor it is necessary to obtain an accurate description of the initial bound state at large momentum values, which is not the case for the pseudostates (see Fig. **??**b) and hence their failure.

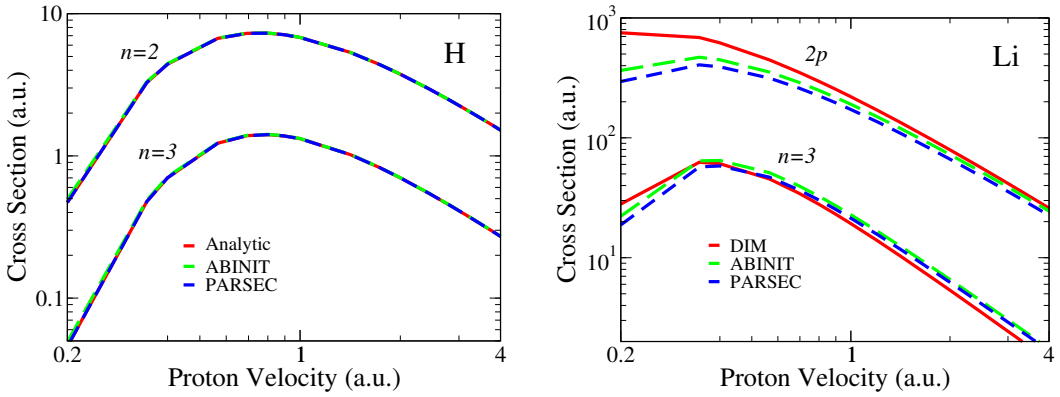

Figure 5: Proton–impact excitation cross section from the ground state for hydrogen and lithium.

3.2 Proton–Impact Ionisation

The transition matrix (**??**) for the proton–impact ionisation of X,

$$\mathrm{H}^+ + X \to \mathrm{H}^+ + X^+ + e^-\,, \tag{18}$$

can also be written in terms of the first order Born approximation. In this case, the final state ψ_f in Eq. (**??**) is an outgoing continuum wavefunction $\psi^-_{\mathbf{k}_f}$ and $\varepsilon_f = k_f^2/2$.

The single–differential proton–impact ionisation cross sections $d\sigma/d\varepsilon_f$ of hydrogen and lithium at a proton velocity of $v_p = 1$ a.u. are shown in Fig. **??**. In the case of hydrogen, the pseudopotential and analytical results agree for all the electron energy range, except at very high values. On the other hand, for lithium, the cross sections computed with pseudopotentials only agree at low energies. Once again, assuming that $\psi^-_{\mathbf{k}_f}(\mathbf{k})$ can be approximated by a plane wave, the form factor is reduced to the Fourier transform of the initial bound state

$$F_{fi}(\mathbf{p}) \sim \widetilde{\psi}_i(\mathbf{p} - \mathbf{k}_f)\,. \tag{19}$$

Then, as k_f increases, so does $p_{\min}$, and the form factor is not well represented by the pseudopotentials. The big discrepancies shown in Fig. **??** provides another demonstration of how a wrong description of the momentum space wavefunction may produce huge errors in collisional processes calculations.

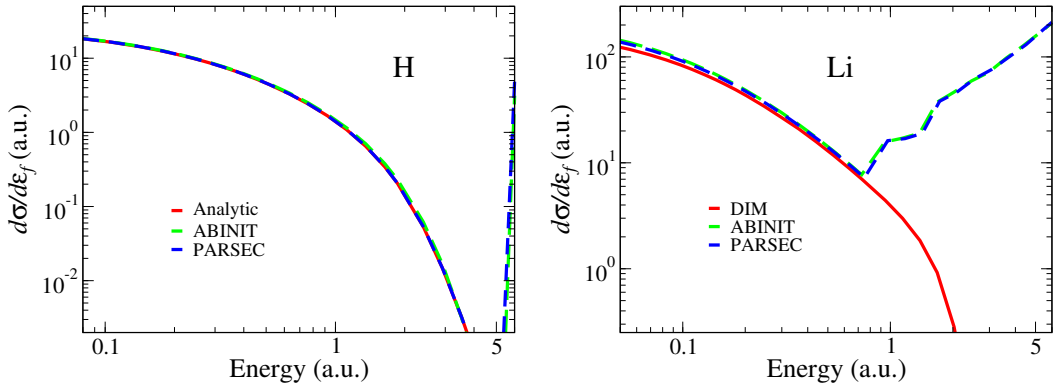

Figure 6: Single differential proton–impact ionisation cross section for hydrogen and lithium at $v_p = 1$ a.u..

3.3 Proton–Impact Charge Exchange

The proton–impact charge exchange of target X is defined as

$$\mathrm{H}^+ + X \to \mathrm{H} + X^+ \,. \tag{20}$$

The charge transfer cross section by the collision of a proton (electron capture) is computed with the first order Brinkman–Kramers approximation [**?**]. Accordingly, the matrix element is defined by

$$T_{fi}^{\mathrm{BK}} = \widetilde{\psi}_f^*(\mathbf{W}_f) \left[\varepsilon_f - \frac{W_f^2}{2} \right] \widetilde{\psi}_i(\mathbf{W}_i) \,, \tag{21}$$

where $\mathbf{W}_i$ and $\mathbf{W}_f$ are the momentum transfer vectors

$$\mathbf{W}_i = W_{i0}\hat{\mathbf{v}} + \boldsymbol{\eta}, \quad W_{i0} = \frac{v}{2} - p_{\min} \tag{22}$$

$$\mathbf{W}_f = W_{f0}\hat{\mathbf{v}} + \boldsymbol{\eta}, \quad W_{f0} = \frac{v}{2} + p_{\min} \,, \tag{23}$$

and they satisfy the condition $\mathbf{W}_i + \mathbf{W}_f = \mathbf{v}$, and $p_{\min}$ is defined in Eq. (**??**).

The charge exchange cross sections of hydrogen and lithium in the ground state are illustrated in Fig. **??**. The cross section of hydrogen is described with high accuracy by the pseudopotential approach for a wide range of proton velocities. However, this process constitutes a symmetrical resonance, i.e. $\varepsilon_f = \varepsilon_i$, and the agreement may be misleading. For the lithium case, the pseudopotentials fail utterly to describe the electron capture correctly at low and high velocities. For low and high v_p values, the momentum transfer vector becomes large and therefore, the cross sections are wrongly calculated with pseudopotentials. The results disagree completely for most of the energy values, except for a very small range of velocities around $v \simeq 0.77$ a.u..

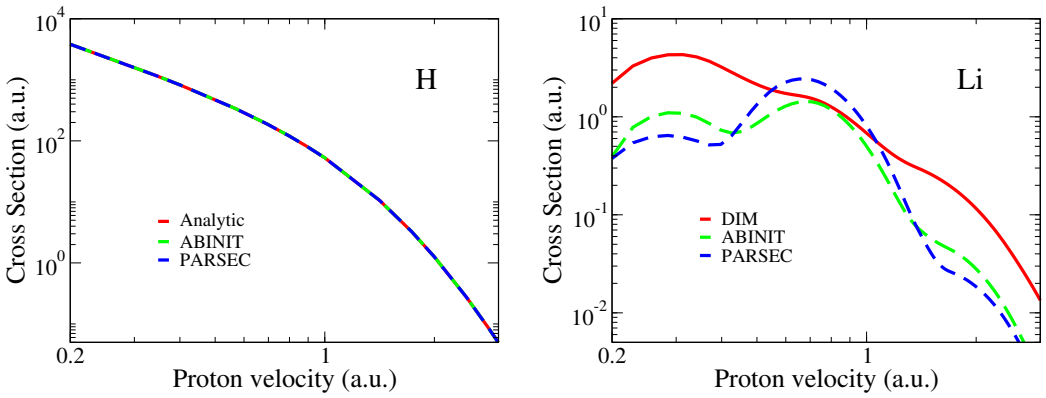

Figure 7: Proton–impact electron capture cross section for hydrogen and lithium.

3.4 Photoionisation

The single photoionisation is defined as

$$\hbar\omega + X \quad \rightarrow \quad X^{+} + e\,. \tag{24}$$

Considering a perturbative photon field, the initial bound ψ_i and final continuum $\psi^{-}_{\mathbf{k}_f}$ states of the target are not considerably distorted; therefore, the relevant matrix element of the photoionisation process is given by

$$T^{\rm Ph}_{\mathbf{k}} = \int \psi^{-}_{\mathbf{k}_f}(\mathbf{r})\,[-i\hat{\boldsymbol{\varepsilon}}_\lambda \cdot \boldsymbol{\nabla}_{\mathbf{r}}]\,\psi_i(\mathbf{r})\,, \tag{25}$$

where $\hat{\boldsymbol{\varepsilon}}_\lambda$ is the polarisation versor and $\mathbf{k}_f = \sqrt{2(\omega + \varepsilon_i)}$, as imposed by the energy conservation.

The first–order photoionisation cross sections of hydrogen and lithium are shown in Fig. **??**. The pseudopotentials results for the hydrogen atom agree with the exact analytical expression results only for low photon energies, failing at larger values. This discrepancies can be understood considering the continuum wavefunction $\psi^{-}_{\mathbf{k}_f}(\mathbf{r})$ as a plane wave. Consequently, the matrix element $T^{\rm Ph}_{\mathbf{k}}$ is reduced to

$$T^{\rm Ph}_{\mathbf{k}} \sim -\,(\hat{\boldsymbol{\varepsilon}}_\lambda \cdot \mathbf{k}_f)\,\widetilde{\psi}_i\,(\mathbf{k}_f)\;, \tag{26}$$

and it is determined entirely by the behaviour of the bound target pseudostate in the momentum representation. For hydrogen, the pseudo–orbital from PARSEC in the Fourier space coincides with the exact analytical solution for the entire range of k, which explains the excellent agreement in the cross section results. For lithium, the pseudopotential cross sections disagree with the DIM results for all energy values. The large oscilations in the cross sections are originated by the spurious oscillatory structure of the bound state for large k values (see inset of Fig. **??**b).

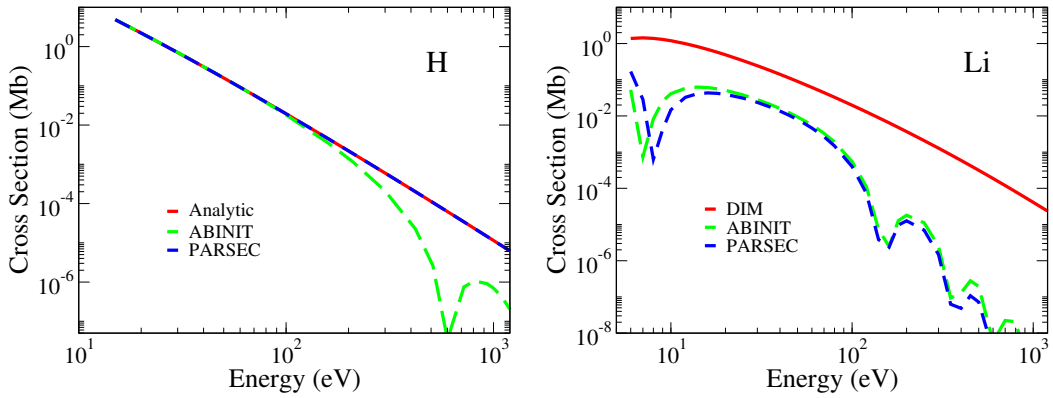

Figure 8: Single photoionisation cross section for hydrogen and lithium.

3.5 DIM photoionisation of many–electron atoms

In order to asses the applicability of the Depurated Inversion Method for atoms with a more complex structure, we compute the photoionisation of many–electron targets with the DIM potentials [**?**] and compare our results with experimental values. The first order photoionisation cross section of nitrogen and neon are shown in Fig. **??**. Experimental data from [**?**, **?**, **?**, **?**] is illustrated with hollow symbols. The DIM photoionisation cross section of these atoms agree excellently with the experimental values for low, medium and high photon–energies. For neon, discrepancies start to be noticeable for low and intermediate energy. An accurate photoionisation description of heavier atoms requires the inclusion of many–body effects that can be relevant, such as orbital relaxation due to the creation of a hole, collective response of inner shell electrons [**?**] and correlation effects.

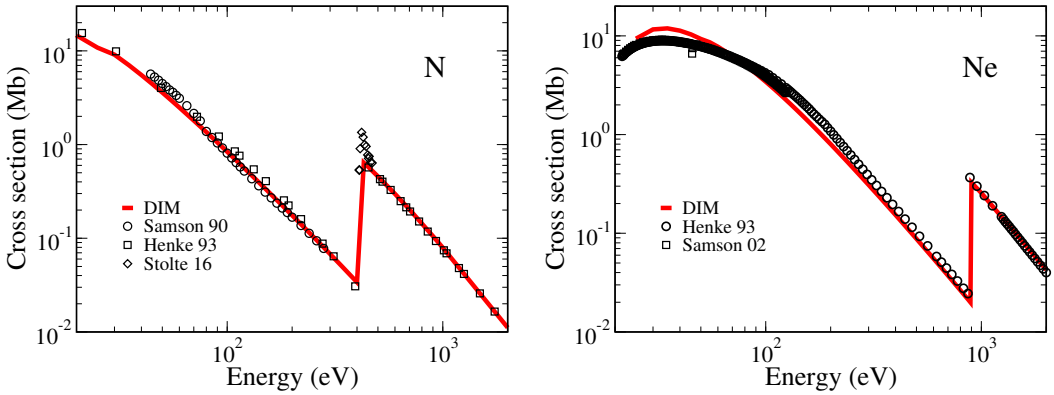

Figure 9: Single photoionisation cross section for nitrogen and neon.

4 Depurated Inversion Method for Molecules

The description of molecular systems constitutes a real challenge due to their generally multicentered and highly non–central nature. Many *ab initio* and semi–empirical theoretical approximations have been developed to this end over the last century.

In this work, the Depurated Inversion Method is extended to determine effective potentials for molecules. In this Section, the theoretical methods are stablished and results for methane are given. Furthermore, collisional processes are computed with these molecular DIM potentials.

4.1 Theory

Without loss of generality, we will present the DIM theoretical grounds for hydride compounds. The Hamiltonian of a N–electron XH_n molecule within the Born–Oppenheimer approximation is given by

$$\mathcal{H} = \sum_{i=1}^{N} \frac{1}{2}\nabla^2_{\mathbf{r}_i} - \sum_{i=1}^{N} \frac{Z_N}{r_i} + \sum_{i=1}^{N} V_H(r_i) + \sum_{i=1}^{N} \frac{1}{r_{ij}} \tag{27}$$

$$V_H(r_i) = -\sum_{j=1}^{n} \frac{1}{|\mathbf{r}_i - \mathbf{R}_{H_j}|} \tag{28}$$

where Z_N is the nuclear charge of the heavier atom and $\mathbf{R}_{H_j}$ are the coordinates of the hydrogens with respect to the X atom. The corresponding Schrödinger equation $\mathcal{H}\Psi = E\Psi$ is solved and the orbitals are expressed as Eq. (**??**) considering the single–center expansion (SCE). The orbitals and energies are found by solving the Hartree–Fock equations. The computation of these equations generally relies on the use of finite basis sets for the representation of the molecular orbitals (MOs). Usually, the MOs are expressed as a linear combination of atomic orbitals (LCAO),

$$\Psi_i = \sum_j c_{ji}\phi_j \,, \tag{29}$$

which can be constructed with Gaussian–type orbitals (GTO) basis sets.

The inverted molecular potential expression, analogous to Eq. (**??**), obtained from GTO basis sets present more difficulties than the atomic case. In addition to the asymptotic divergences and the poles, large unphysical oscillations arise [**?**, **?**, **?**, **?**]. These big oscillations are originated from imperceptible undulations present in the MOs due to the finite number of the basis set. The second derivative, necessary to evaluate the invertion formula, amplifies these features [**?**, **?**]. The appearance of these oscillations in the inverted potentials forces us to incorporate further actions in the depuration scheme. To illustrate this procedure, we consider the $1s$ orbital of the carbon atom. We solved the Hartree–Fock equations using the 6-311G basis set with GAMESS code [**?**, **?**]. We obtain the inverted potentials by implementing Eq. (**??**). The resulting $Z_{1s}^{\text{6-311G}}$ charge is shown in Fig. **??**a with a dot–dashed line. The charge oscillates significantly at low distances and diverges for higher r values. The same calculation was repeated using the universal Gaussian basis set (UGBS), which has a more significant amount of primitives. The corresponding inverted charge Z_{1s}^{UGBS} is exhibited in the figure with a dashed line. Although the charge still diverges around $r \approx 1$ a.u., the oscillations are now circumscribed near the nucleus. Finally, the differential Hartree–Fock equations for the carbon atom were solved using the finite–differences (FD) method. The $1s$ inverted charge obtained with this procedure, Z_{nl}^{FD}, shows no oscillations since no basis sets have been used to construct the orbital; however, the charge still diverges for $r > 1$ a.u., as it usually does for all HF calculations.

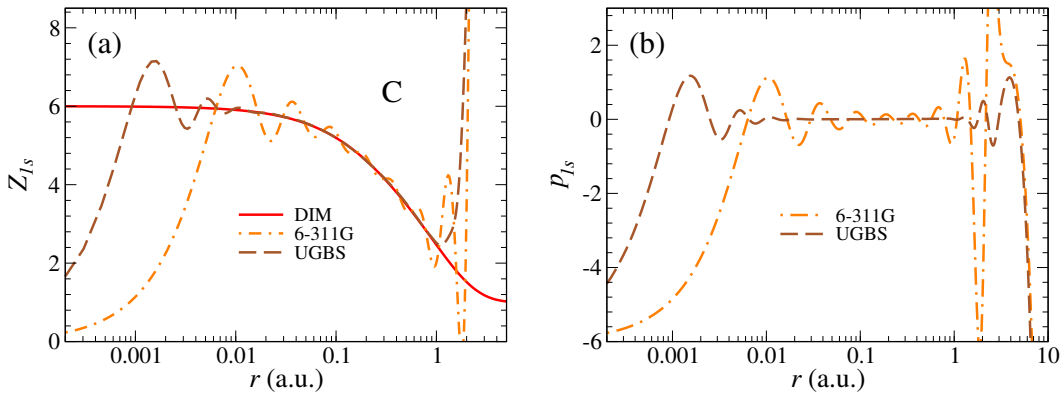

Figure 10: (a) Effective charges for the $1s$ orbital of carbon. (b) Basis–set oscillation profiles.

As shown in the figure, for each basis set used in the calculations, different oscillation profiles will arise, which are defined as

$$p_{nl}^{\rm BS} = Z_{nl}^{\rm BS} - Z_{nl}^{\rm FD}\,, \tag{30}$$

where $Z_{nl}^{\rm BS}$ is the inverted charge of the atom using the particular basis set "BS" and $Z_{nl}^{\rm FD}$ is the effective charge obtained from the invertion of the finite–difference wavefunctions. In the previous example, the basis set considered for calculating the $1s$ orbital of carbon were 6-311G and UGBS. The oscillation profiles for the $1s$ orbital, using Eq. (**??**) for these basis sets, are shown in Fig. **??**b. Since the orbital profiles for each atomic basis set are distinctive, once they are determined for the atomic case, they can be removed in further molecular calculations. An example of this procedure is given in the following Section.

4.2 Example: Methane

In order to illustrate the implementation of the DIM for molecules, we considered the methane molecule, which has a suitable spherical geometry. We computed the HF molecular orbitals and energies of CH_4 employing the UGBS basis sets of carbon and hydrogen, using the GAMESS code. The charges obtained by direct inversion are given in Fig. **??** with dashed lines. Since the molecular orbitals are given by LCAO of carbon and hydrogen, the oscillations of the inverted charges are a consequence of the finite basis set of these atoms. To remove the most important oscillations it is necessary to determine the oscillation profiles produced by the atomic carbon basis set. We use Eq. (**??**) to determine the $p_{1s}^{\rm UGBS}$, $p_{2s}^{\rm UGBS}$ and $p_{2p}^{\rm UGBS}$ profiles of carbon. Then, we remove the oscillations by substracting the carbon $p_{nl}^{\rm UGBS}$ profiles to the corresponding inverted charges $Z_i^{\rm UGBS}$ of CH_4. The oscillations are removed for all orbitals except for the $2a_2$, which presents small oscillatory residues from the hydrogen basis set. Since the residual fluctuations are very small and near the nucleus, we proceeded to implement the depuration scheme as described in Section **??**. We define a new parametric DIM charge equation,

$$Z(r) = \sum_j Z_j e^{-\alpha_j r} + Z_{\rm H} e^{-(\ln r - \ln \beta)^2/(2\gamma)} + 1\,. \tag{31}$$

In contrast to the approximation proposed for atoms (**??**), a second term has been added to the formula to account for the presence of the hydrogens. The optimised parameters for the methane molecule are given in Table **??** and the corresponding DIM charges are shown in Fig. **??**, with solid lines. The orbital energies obtained with these charges are also given in the table.

nl	E	Z	α	β	γ
$1a_1$	-11.1949	1.925280	0.641982		
		0.953120	5.571510		
		2.121600	1.500440		
$2a_2$	-0.9204	2.912200	3.149990		
		2.087800	0.771371		
		1.23640		2.329570	0.053420
$2t_1$	-0.5042	0.901953	2.895140		
		1.112030	0.388649		
		2.986017	2.931210		
		1.30182		2.169850	0.012616

Table 1: Energies and fitting parameters for the DIM effective charges (Eq. (**??**)), for CH_4.

4.3 Collisional processes

The orientation of the molecular targets are important for determining the cross sections of collisional processes. However, the molecular orientations in most collisional experiments are generally not pre–established. Thus, the spherical averaged description of the system, assumed by the DIM potential is a

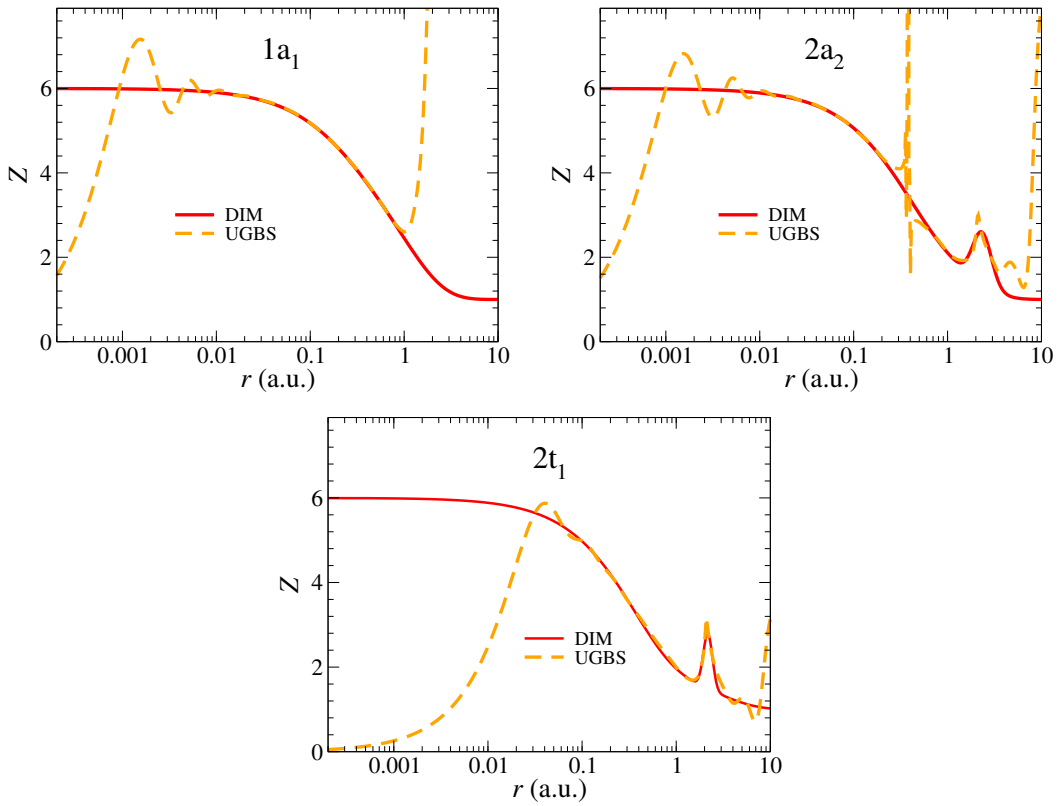

Figure 11: Effective charges of CH_4; direct inversion (dashed line) and depurated inverted (solid line).

valid approximation. In the following, we examine two collisional processes in the first–order approximation: proton–impact ionisation and single photoionisation.

4.3.1 Proton–Impact Ionisation

Results for the proton–impact ionisation cross section for CH_4, calculated under the first Born approximation, are given in Fig. **??**. Experimental data from Ref. [**?**, **?**] are displayed with symbols. The initial bound and the final continuum states of the molecule needed for the T–matrix computation (Eq. (**??**)) were calculated with the DIM potentials from Section **??**. The photoionisation cross section for high and intermediate energies shows good agreement with the experimental results. The failure at low energies is attributed to the validity of the first Born approximation and not to our DIM approach.

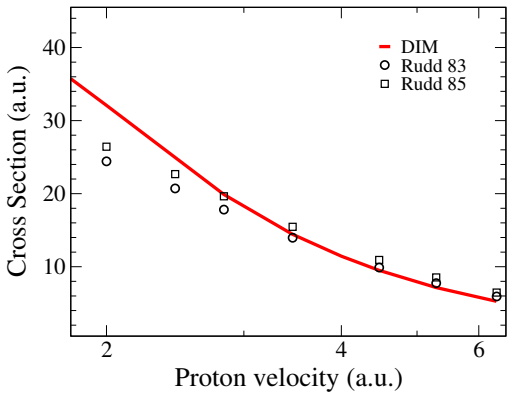

Figure 12: Proton–impact ionisation cross section for CH_4. Solid line: first–order DIM theoretical calculations. Symbols: experiments from Ref. [**?**, **?**].

4.3.2 Photoionisation

The photoionisation cross section for CH_4, calculated with the DIM potentials in a first order approximation, is shown in Fig. **??** (solid lines). Good agreement with the experimental results (symbols) is found for high energy values and at the thresholds. The curve between ∼15 and ∼300 eV shows the photoionisation from the outer $n = 2$ shell. The pronounced discontinuity at 300 eV corresponds to the threshold of the $1a_1$ inner shell orbital. For low and intermediate photon–energies, the agreement between our calculations and the experimental values from Ref. [**?**, **?**, **?**] is not perfect. Phenomena such as molecular orbital relaxation, possible collective contributions and correlation effects must be considered in further calculations. On the other hand, for the $1a_1$ inner shell photoionisation, these effects are not significant and we obtain a perfect agreement with the experimental results.

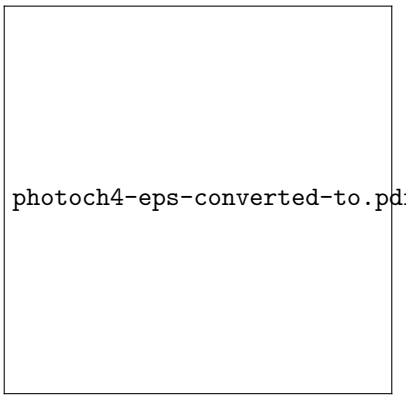

Figure 13: Single photoionisation cross section of CH_4. Solid line: first–order DIM theoretical calculations. Symbols: experiments from Ref. [**?**, **?**, **?**].

5 Concluding remarks

In this work, we explored the possibility of using pseudopotentials within the single electron model to calculate inelastic transitions. The first Born approximation was used to calculate proton–impact excitation, ionization, electron capture and photoionization. Two simple atoms were studied, having a single electron in the outer shell. For hydrogen, we found great agreement for all the collisional processes, for low and intermediate energies. In the case of lithium, the only process that can be calculated with a reasonable accuracy is the proton–impact excitation. We concluded that the range of validity is restrained

to very small momentum transfers. The Depurated Inversion method, on the other hand, accurately reproduce photoionisation experimental results for many–electron atoms.

We extended the DIM for molecular systems. In this case, the inversion procedure raises huge oscillation due the finite size of the basis involved in the Hartree–Fock orbital calculations. An additional step is included during the depuration scheme. In order to determine the oscillation profile for a particular basis set, we computed the atomic inverted charges also in a finite–differences framework. By substracting the charges, it is possible to isolate the oscillations corresponding to this particular basis set. We used the DIM method to determine the effective potentials for CH_4. These potentials are implemented in a first–order proton–impact ionisation and photoionisation cross sections calculations. For both processes, we found very good agreement with the experimental results. The main discrepancies can be attributed to the fact that only first–order is considered in the perturbation theory.

Acknowledgement

The authors thank the Consejo Nacional de Investigaciones Científicas y Técnicas (CONICET), Universidad de Buenos Aires (UBA) and Agencia Nacional de Promoción Científica y Tecnológica (ANPCyT) for the grants that supported this work.

References

[1] `https://parsec.ices.utexas.edu/styled-2/`

[2] J. R. Chelikowsky, N. Troullier, and Y. Saad, Finite–difference–pseudopotential method: Electronic structure calculations without a basis, Phys. Rev. Lett. **72**, 1240–1243 (1994).

[3] A. M. P. Mendez, Método de Inversión Depurada para Potenciales Locales en Átomos y Moléculas, Tesis de Licenciatura, Universidad Nacional de Salta (2015).

[4] A. M. P. Mendez, D. M. Mitnik, and J. E. Miraglia, Depurated inversion method for orbital–specific exchange potentials. Int. J. Quantum Chem. **116**, 24 (2016).

[5] A. M. P. Mendez, D. M. Mitnik, and J. E. Miraglia, Local Effective Hartree–Fock Potentials Obtained by the Depurated Inversion Method, Advances in Quantum Chemistry **76**, 117–132 (2018).

[6] `https://www.abinit.org/psp-tables`

[7] D. R. Hamann, M. Schlüter, and C. Chiang, Norm–Conserving Pseudopotentials, Phys. Rev. Lett. **43**, 1494–1497 (1979).

[8] C. Froese Fischer, T. Brage, and P. Jönsson, *Computational atomic structure: an MCHF approach*, Institute of Physics Publishing (1997).

[9] W. R. Johnson, *Atomic structure theory : lectures on atomic physics*, Springer (2007).

[10] Von H. C. Brinkman and H. A. Kramers, Zur Theorie der Einfangung von Elektronen durch α–Teilchen. Proc. K. Akad. van Wet. **33**, 973–984 (1930).

[11] B. L. Henke, E. M. Gullikson, and J. C. Davis, X–Ray Interactions: Photoabsorption, Scattering, Transmission, and Reflection at E=50–30000 eV, Z=1–92, At. Data Nucl. Data Tables **54**, 181–342 (1993).

[12] J. A. R. Samson and G. C. Angel, Single– and double–photoionization cross sections of atomic nitrogen from threshold to 31 Å, Phys. Rev. A **42**, 1307–1312 (1990).

[13] J. A. R. Samson and W. C. Stolte, Precision measurements of the total photoionization cross–sections of He, Ne, Ar, Kr, and Xe, J. Electron Spectros. Relat. Phenomena **123**, 265–276 (2002).

[14] W. C. Stolte, V. Jonauskas, D. W. Lindle, M. M. Sant'Anna, and D. W. Savin, Inner–shell Photoionization studies of neutral atomic nitrogen, Astrophys. J. **818**, 149 (2016).

[15] D. L. Ederer, Photoionization of the $4d$ electrons in Xenon, Phys. Rev. Lett. **13**, 760–762 (1964).

[16] P. R. T. Schipper, O. V. Gritsenko, and E. J. Baerends, Kohn-Sham potentials corresponding to Slater and Gaussian basis set densities, Theor. Chem. Accounts: Theory, Comput. Model. (Theoretica Chim. Acta) **98**, 16–24 (1997).

[17] M. E. Mura, P. J. Knowles, and C. A. Reynolds, Accurate numerical determination of Kohn–Sham potentials from electronic densities: I. Two–electron systems, J. Chem. Phys. **106**, 9659–9667 (1997).

[18] C. R. Jacob, Unambiguous optimization of effective potentials in finite basis sets, J. Chem. Phys. **135**, 244102 (2011).

[19] A. P. Gaiduk, I. G. Ryabinkin, and V. N. Staroverov, Removal of Basis–Set Artifacts in Kohn–Sham Potentials Recovered from Electron Densities, J. Chem. Theory Comput. **9**, 3959–3964 (2013).

[20] M. W. Schmidt, K. K. Baldridge, J. A. Boatz, S. T. Elbert, M. S. Gordon, J. H. Jensen, S. Koseki, N. Matsunaga, K. A. Nguyen, S. Su, T. L. Windus, M. Dupuis, and J. A. Montgomery, General atomic and molecular electronic structure system, J. Comput. Chem. **14**, 1347–1363 (1993).

[21] M. S. Gordon and M. W. Schmidt, Advances in electronic structure theory: GAMESS a decade later, in Theory Appl. Comput. Chem., **41**, 1167–1189 (2005).

[22] M. E. Rudd, R. D. DuBois, L. H. Toburen, C. A. Ratcliffe, and T. V. Goffe, Cross sections for ionization of gases by 5–4000 keV protons and for electron capture by 5–150 keV protons, Phys. Rev. A **28**, 3244–3257 (1983).

[23] M. E. Rudd, Y. K. Kim, D. H. Madison, and J. W. Gallagher, Electron production in proton collisions: total cross sections, Rev. Mod. Phys. **57**, 965–994 (1985).

[24] A. P. Lukirskii, I. A. Brytov, and T. M. Zimkina, Optika i spektr. **17**, 234 (1964).

[25] B. L. Henke, P. Lee, T. J. Tanaka, R. L. Shimabukuro, and B. K. Fujikawa, Low–energy X–ray interaction coefficients: Photoabsorption, scattering, and reflection: E=100–2000 eV Z=1–94, At. Data Nucl. Data Tables **27**, 1–144 (1982).

[26] J. A. R. Samson, G. N. Haddad, T. Masuoka, P. N. Pareek, and D. A. L. Kilcoyne, Ionization yields, total absorption, and dissociative photoionization cross sections of CH4 from 110 to 950 Å, J. Chem. Phys. **90**, 6925–6932 (1989).